The boundaries of the West African craton, with special reference to the basement of the Moroccan metacratonic Anti-Atlas belt

Nasser Ennih and Jean-Paul Liégeois

Geological Society, London, Special Publications 2008; v. 297; p. 1-17
doi:10.1144/SP297.1

The boundaries of the West African craton, with special reference to the basement of the Moroccan metacratonic Anti-Atlas belt

NASSER ENNIH[1] & JEAN-PAUL LIÉGEOIS[2]

[1]*Geodynamic Laboratory, El Jadida University, BP. 20, 24000, El Jadida, Morocco (e-mail: ennih@ucd.ac.ma)*

[2]*Isotope Geology, Royal Museum for Central Africa, B-3080 Tervuren, Belgium (e-mail: jean-paul.liegeois@africamuseum.be)*

Abstract: The West African craton (WAC) was constructed during the Archaean and the *c.* 2 Ga Palaeoproterozoic Eburnian orogeny. Mesoproterozoic quiescence at *c.* 1.7–1.0 Ga allowed cratonization. In the absence of Mesoproterozoic activity, there are no known WAC palaeogeographical positions for that time. At the beginning of the Neoproterozoic, the WAC was affected by several extensional events suggesting that it was subjected to continental breakup. The most important event is the formation of the Gourma aulacogen in Mali, and the Taoudeni cratonic subcircular basin and deposition of platform sediments in the Anti-Atlas. At the end of the Neoproterozoic, the WAC was subjected to convergence on all its boundaries, from the north in the Anti-Atlas, to the east along the Trans-Saharan belt, to the south along the Rockelides and the Bassarides and to the east along the Mauritanides. This led to a partial remobilization of its cratonic boundaries giving rise to a metacratonic evolution. The WAC boundaries experienced Pan-African Neoproterozoic to Early Cambrian transpression and transtension, intrusion of granitoids and extrusion of huge volcanic sequences in such as in the Anti-Atlas (Ouarzazate Supergroup). Pan-African tectonism generated large sediment influxes around the WAC within the Peri-Gondwanan terranes whose sedimentary sequences are marked by distinctive zircon ages of 1.8–2.2 Ga and 0.55–0.75 Ga.

WAC rocks experienced Pan-African low grade metamorphism and large movements of mineralizing fluids. In the Anti-Atlas, this Pan-African metacratonic evolution led to remobilization of REE in the Eburnian granitoids due to the activity of F-rich fluids linked to extrusion of the Ouarzazate Supergroup. During the Phanerozoic, the western WAC boundary was subjected to the Variscan orogeny, for which it constituted the foreland and was, therefore moderately affected, showing typical thick-skin tectonics in the basement and thin-skin tectonics in the cover. During the Mesozoic, the eastern and southern boundaries of the WAC were subjected to the Atlantic opening including Jurassic dolerite intrusion and capture of its extreme southern tip by South America. The Jurassic is also marked by the development of rifts on its eastern and northern sides (future Atlas belt). Finally, the Cenozoic period was marked by the convergence of the African and European continents, generating the High Atlas range and Cenozoic volcanism encircling the northern part of the WAC. The northern metacratonic boundary of the WAC is currently uplifted, forming the Anti-Atlas Mountains.

The boundaries of the WAC, metacratonized during the Pan-African orogeny have been periodically rejuvenated. This is a defining characteristic of the metacratonic areas: rigid, stable cratonic regions that can be periodically cut by faults and affected by magmatism and hydrothermal alteration – making these areas important for mineralization.

A craton is a stable part of the continental lithosphere which has not been deformed for a long time (Bates & Jackson 1980). Although cratons are not tectonically active, they can be located near active margins, such as the Brazilian craton at the rear of the Andean active margin. Cratons proximal to collision zones act as a shield, as their thick lithosphere protects them from most of the collisional effects (Black & Liégeois 1993). However, cratons can be partly subducted or affected by transpressive tectonics. Such partial reactivation of a rigid body or of the boundaries of a rigid body gives rise to geological characteristics different from the cratonic quiescence as well as from the intense activity occurring in a mobile belt. This has been called *metacratonic evolution* (Abdelsalam *et al.* 2002).

This special volume has been generated by the UNESCO IGCP485 (International Geological Correlation Programme, now International Geoscience Programme) called *Cratons, metacratons and mobile belts: keys from the West African craton boundaries; Eburnian versus Pan-African signature, magmatic, tectonic and metallogenic*

From: ENNIH, N. & LIÉGEOIS, J.-P. (eds) *The Boundaries of the West African Craton.* Geological Society, London, Special Publications, **297**, 1–17.
DOI: 10.1144/SP297.1 0305-8719/08/$15.00

implications. The aim of this project, and of this book, was to encompass the whole evolution of the boundaries of the West African craton, from the Archaean/Palaeoproterozoic towards Recent times. The IGCP485 organized field conferences in remote areas such as the Reguibat Rise in Mauritania, the Gourma region in Mali, the Hoggar shield in Algeria and twice in the Anti-Atlas belt in Morocco. This book contains twenty-four papers concerning these regions and other boundaries of the West African craton.

The West African craton

The West African craton (WAC) is composed of three Archaean and Palaeoproterozoic metamorphic and magmatic shields separated by two cratonic sedimentary basins (Fig. 1). The WAC components include: to the south the Man shield, to which the smaller Kayes and Kenieba inliers can be associated; to the north the Reguibat shield; and to the extreme north, the Anti-Atlas belt. In between are, in the centre, the huge Taoudeni basin and to the north the Tindouf basin. The Man and Reguibat shields comprise Archaean nuclei to the west (Feybesse & Milési 1994; Potrel *et al.* 1998; **Key *et al.***). In the Man shield, a large part of the WAC consists of the Palaeoproterozoic Birimian continent (Abouchami *et al.* 1990; Liégeois *et al.* 1991; Boher *et al.* 1992; **Soumaila *et al.***). The Reguibat shield contains Palaeoproterozoic assemblages in the eastern part as well as Archaean components that include kimberlites (**Kahoui *et al.***). The Anti-Atlas belt comprises only a Palaeoproterozoic basement (Thomas *et al.* 2004). The WAC terranes were affected by the Eburnian orogeny, at around 2 Ga. During the Mesoproterozoic, no event or rocks are known in the WAC. This extremely quiet period between 1.7 Ga and 1 Ga allowed this large area to become a craton by acquiring a thick lithosphere (Black & Liégeois 1993). The palaeoposition of the WAC during the Mesoproterozoic is not known. By contrast to the Mesoproterozoic, the Neoproterozoic was an important period of evolution for the West African craton. At the beginning of the Neoproterozoic, the WAC was affected by several extensional events associated with continental breakup. The most important event was the formation of the Gourma aulacogen in Mali (Moussine-Pouchkine & Bertrand-Sarfati 1978) but also the deposition of passive margin sediments on its

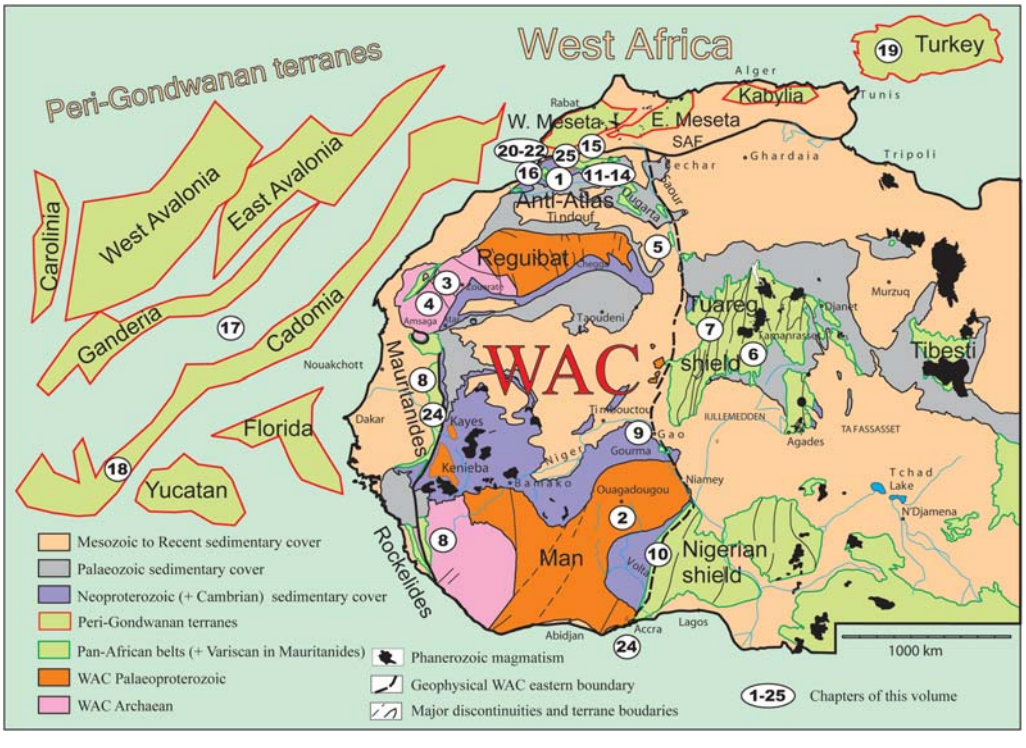

Fig. 1. Main geological units in West Africa, from Fabre (2005) and Liégeois *et al.* (2005). The positions and shapes of the Peri-Gondwanan terranes are based on **Nance *et al.***

northern boundary in the Anti-Atlas (Bouougri & Saquaque 2004) and to the SE in the Voltas basin (Ako & Wellman 1985; Nédélec *et al.* 2007). The formation of the huge Taoudeni cratonic subcircular basin also began during that period (Bronner *et al.* 1980).

At the end of the Neoproterozoic, the WAC was first subjected to island arc accretion during 760–660 Ma on its northern and eastern sides, in the Moroccan Anti-Atlas (Thomas *et al.* 2002; Samson *et al.* 2004; D'Lemos *et al.* 2006; **Bousquet *et al.***), in the Malian Tilemsi (Caby *et al.* 1989) and in the Gourma area (De la Boisse 1979). During the main Pan-African orogenic phase, the WAC was subjected to convergence on all its boundaries, from the north in the Anti-Atlas (Hefferan *et al.* 2000; Ennih & Liégeois 2001), to the east along the Trans-Saharan belt (Black *et al.* 1979, 1994; Affaton *et al.* 1991; **Attoh & Nude**), to the south with the Rockelides and the Bassarides belts and to the east with the Mauritanides belt (**Villeneuve**), with several thrust sheets preserved on the craton itself, such as in Mali (**Caby *et al.***). These collisions partly remobilized other cratonic regions to the east of the WAC in the Tuareg shield (Liégeois *et al.* 2003; **Bendaoud *et al.*; Adjerid *et al.***) and also the peri-Gondwanan terranes (**Nance *et al.*; Pereira *et al.*; Gürsu & Gonçuoğlu**).

The boundaries of the West African craton

The Pan-African orogeny induced a partial remobilization of the WAC boundaries, inducing a metacratonic evolution. At the end of the Neoproterozoic, the West African craton belonged to the subducting plate, implying that it was never an active margin above a subduction oceanic plate (Black *et al.* 1979; Hefferan *et al.* 2000; Ennih & Liégeois 2001; **Villeneuve**), with craton-ward directed fold-and-thrust structures (Jahn *et al.* 2001; **Caby *et al.***) also forming outboard of the craton (**Attoh & Brown**). The West African craton acted as a rigid indenter during the Pan-African orogeny in a similar way as India is currently indenting the Asian continent (Black *et al.* 1979). The thick cratonic continental lithosphere was partly affected by transpression and transtension tectonic episodes, intrusion of granitoids and extrusion of volcanic sequences, such as in the Anti-Atlas (Ouarzazate Supergroup). High temperature/low pressure grade metamorphism occurred with large movements of fluids causing mineralization in several areas (Inglis *et al.* 2004; **Kolb *et al.*; Belkabir *et al.***). Although partially buried by younger deposits, rock exposures contain excellent preservation of the early Neoproterozoic events such as the passive margin sediments (Bouougri & Saquaque 2004), the early thrust oceanic terranes (Samson *et al.* 2004; **Bousquet *et al.***) and Pan-African magmatism (**Touil *et al.*; Ezzouhairi *et al.***). The Pan-African orogeny generated large sediment influx, for example outside the WAC, within the Peri-Gondwanan terranes whose sedimentary sequences are marked by the WAC-typical signature, a bimodal set of zircon ages at *c.* 1.8–2.2 Ga and at 0.55–0.75 Ga (**Nance *et al.***). The metacratonic evolution affected some parts of the WAC and peri-Gondwanan terranes such as the *c.* 2 Ga Icartian gneisses in Brittany (Calvez & Vidal 1978; Samson & D'Lemos 1998). A better knowledge of the boundaries of the West African craton is, therefore, of importance for the study of peri-Gondwanan terranes in Europe and in America.

During the latest Neoproterozoic and early Palaeozoic, the western WAC boundaries were first subjected to a major extensional event producing sedimentary and volcanic sequences (**Alvaro *et al.*; Pouclet *et al.***) and the drifting of some of the peri-Gondwanan terranes (**Nance *et al.***). Thick Phanerozoic sedimentary sequences were deposited afterwards up to Devonian times (**Baidder *et al.*; Ouanaimani & Lazreq**). The Late Palaeozoic Variscan orogeny moderately affected the WAC by generating thick-skin tectonics in the basement and thin-skin tectonics in the sedimentary cover rocks (Caritg *et al.* 2004; Burkhard *et al.* 2006; **Baidder *et al.*; Dabo *et al.*; Soulaimani & Burkhard**). In the Mesozoic, the western and southern WAC boundaries were subjected to the Atlantic rifting and Jurassic dolerite intrusions and massive Central Atlantic magmatic province (CAMP) basalt flows (Marzoli *et al.* 1999; Deckart *et al.* 2005; Verati *et al.* 2005). The Jurassic was also marked by the development of rifts on the eastern side (e.g. Gao rift) and on the northern side (e.g. Atlas belt), contemporaneously with the development of the Central Atlantic Ocean and the Western Mediterranean Sea (Laville *et al.* 2004; Guiraud *et al.* 2005). Finally, the Cenozoic era was marked by the convergence of the African and European continents, generating the High Atlas range, the uplift of the Anti-Atlas (Malusa *et al.* 2007) and the Cenozoic volcanism in West Africa (**Berger *et al.***) and the Hoggar (Liégeois *et al.* 2005). The northern metacratonic boundary of the WAC is currently uplifted, forming the Anti-Atlas Mountains.

The boundaries of the WAC, metacratonized during the Pan-African orogeny, have been rejuvenated periodically. The rigid WAC metacraton has been affected by the reactivation of lithospheric faults that facilitate hydrothermal mineralization (Pelleter *et al.* 2007). This is the main characteristic

of the metacratonic areas (Liégeois *et al.* 2003, 2005): being rigid but affected by faults of lithospheric scale, they constitute areas subjected to reactivation, including intraplate reactivations (Azzouni-Sekkal *et al.* 2003; Liégeois *et al.* 2005), making them areas likely to be rich in mineralizations.

The case study of the remobilization of the Eburnian basement in the Anti-Atlas belt

Our recent study on the Eburnian basement of the Anti-Atlas, in the Zenaga inlier (Figs 2 and 3) has revealed extensive REE mobility in Eburnian granites during the Pan-African orogeny. REE mobility is attributed to Pan-African transcurrent tectonism and associated Neoproterozoic Ouarzazate Supergroup volcanism.

The Anti-Atlas belt

The Anti-Atlas belt (Fig. 2) is separated in two parts by the Anti-Atlas major fault (AAMF) – long considered as the northern limit (e.g. Hefferan *et al.* 2000) of the WAC because it is marked by ophiolitic remnants, including that of Bou Azzer, and because Eburnian outcrops are not known north of it in the Saghro Mountains. For various geological but also rheological and isotopic reasons, Ennih & Liégeois (2001) proposed that the actual northern boundary of the WAC is the South Atlas fault that borders the High Atlas mountain range to the south (Fig. 2) of the AAMF. According to Ennih & Liégeois (2001), the South Atlas Fault marks the edge of the deepening of the WAC basement under Neoproterozoic volcano-sedimentary series. Here we will focus on the Zenaga inlier, which consists of Eburnian basement rocks and is located just to the south of the AAMF, for deciphering the Pan-African effects on the WAC northern boundary basement.

The Zenaga inlier

The Zenaga inlier is a depression of about 500 km^2 containing mainly Palaeoproterozoic gneisses and granitoids unconformably overlain by the late Neoproterozoic Ouarzazate volcanic Supergroup or by the Cambrian Tata Group (Fig. 3). Within the inlier, Neoproterozoic rocks also consist of passive margin sediments (Taghdout Group), pre-Pan-African doleritic dykes and sills and a late Pan-African alkaline ring-complex. Along the AAMF, to the west and to the east, remnants of the Bou Azzer–Sirwa oceanic terrane are present. A summary of the geology of the area helps to understand the metacratonic evolution of the Zenaga basement.

The Zenaga Palaeoproterozoic metamorphic rocks include medium to high-grade amphibolite facies grey gneisses, biotite-rich schists, garnet $\pm$ sillimanite paragneisses, calc-silicate rocks, migmatites and rare amphibolites. The gneissic layering and the migmatitic leucosomes are deformed by isoclinal ductile folds, whose axes have variable plunge. This basement represents a high-grade metamorphic supracrustal series. These schists have not been dated but inherited zircons at *c.* 2170 Ma within the *c.* 2035 Ma cross-cutting granitoids could be attributed to the Zenaga schists (Thomas *et al.* 2002).

The Zenaga Palaeoproterozoic granitoids are represented by the Azguemerzi mesocratic granodiorite, and the Aït Daoui, Assersa, Tamarouft and Tazenakht granites. The Zenaga plutons show quartzo-feldspathic layers separated by biotite and garnet layers, locally associated with gneisses and anatectic products. They contain rare metasedimentary xenoliths and no mafic microgranular enclaves (MME). The presence of aluminous minerals (biotite, garnet, muscovite), the association with migmatitic rocks, the absence of MME suggest that the Zenaga granitoids originated by the partial melting of crustal rocks. The granodiorite and the granites have been dated at 2037 $\pm$ 7 Ma, 2037 $\pm$ 9 Ma and 2032 $\pm$ 5 Ma (U–Pb zircon ages, Thomas *et al.* 2002). These dates give a minimum age for the gneisses and schists.

The Zenaga granitoid basement is unconformably covered by the Taghdout sedimentary Group, also known as the Tizi n-Taghatine Group (Thomas *et al.* 2004). The Taghdout Group displays brittle tectonic faults folds associated with a south-verging thrust event. Portions of this unit have been metamorphosed to greenschist facies. The Taghdout Group contains well-preserved sedimentary features, such as ripple marks, desiccation cracks or oblique stratification (Bouougri & Saquaque 2004). The Taghdout Group is a 2 km-thick succession deposited during three stages of an extensional event (Bouougri & Saquaque 2004): (1) a shallow-water and gently dipping mixed siliciclastic–carbonate ramp facing north and attached to braided alluvial plain in the south, indicating a relatively stable margin; (2) tholeiitic sills and dykes of the Ifzwane Group that cut the sedimentary sequence and the basement of the Zenaga inlier (particularly to the NW; Fig. 3a); (3) deepening of the margin marked by turbidites.

Although they are not directly in contact with the Zenaga basement, remnants of the Bou Azzer and Sirwa oceanic island arc complex occur along the AAMF (Fig. 2). This complex comprises ophiolitic sequences in which plagiogranites have been

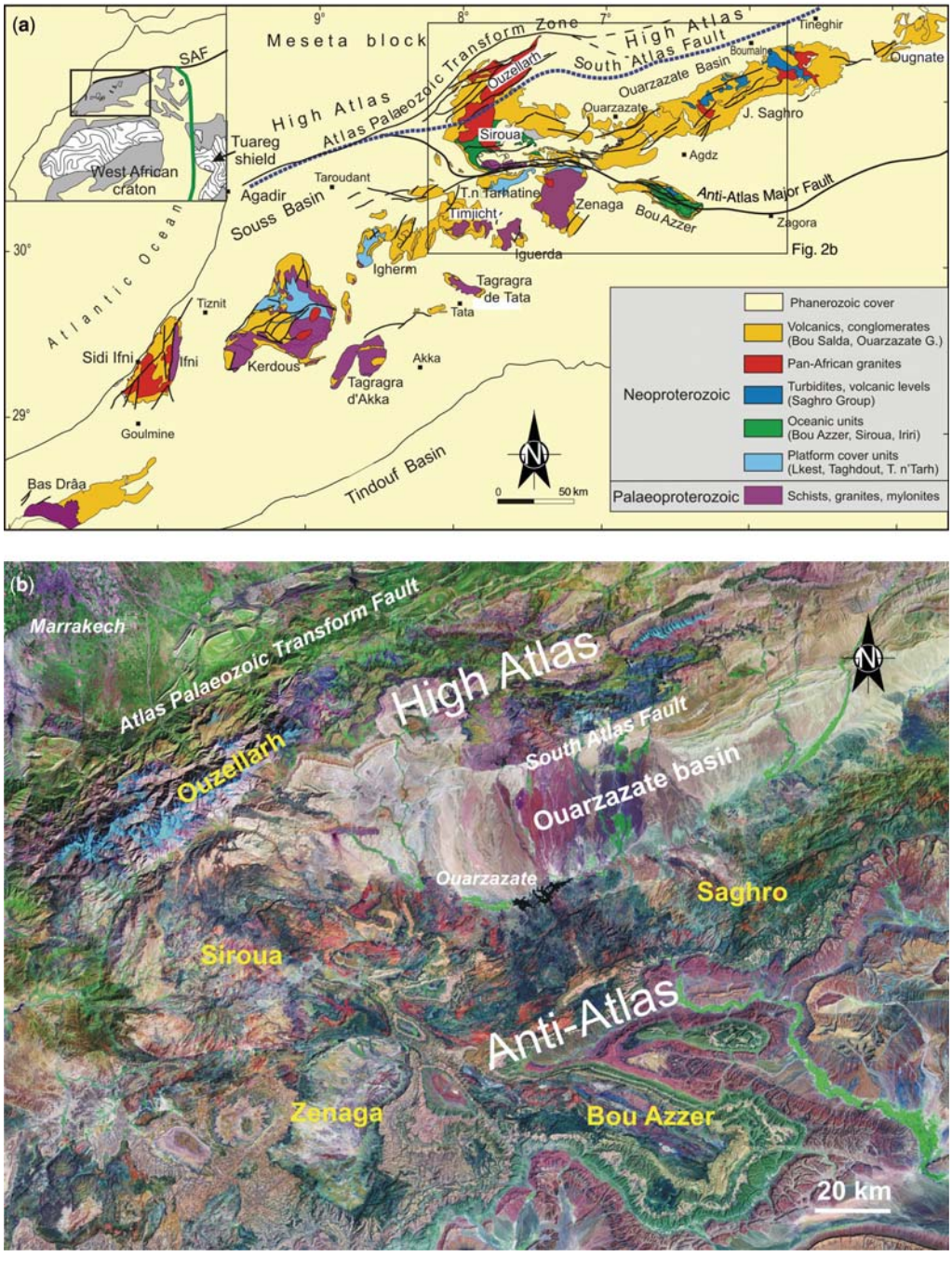

Fig. 2. (**a**) Geological map of the Anti-Atlas (Morocco), from Thomas *et al.* (2004) and Gasquet *et al.* (2008). The rectangle outlines the area in Figure 1B. (**b**) Satellite photograph of the Anti-Atlas (Orthorectified Landsat Thematic Mapper Mosaics as compressed colour imagery in MrSIDTM file format from Lizardtech).

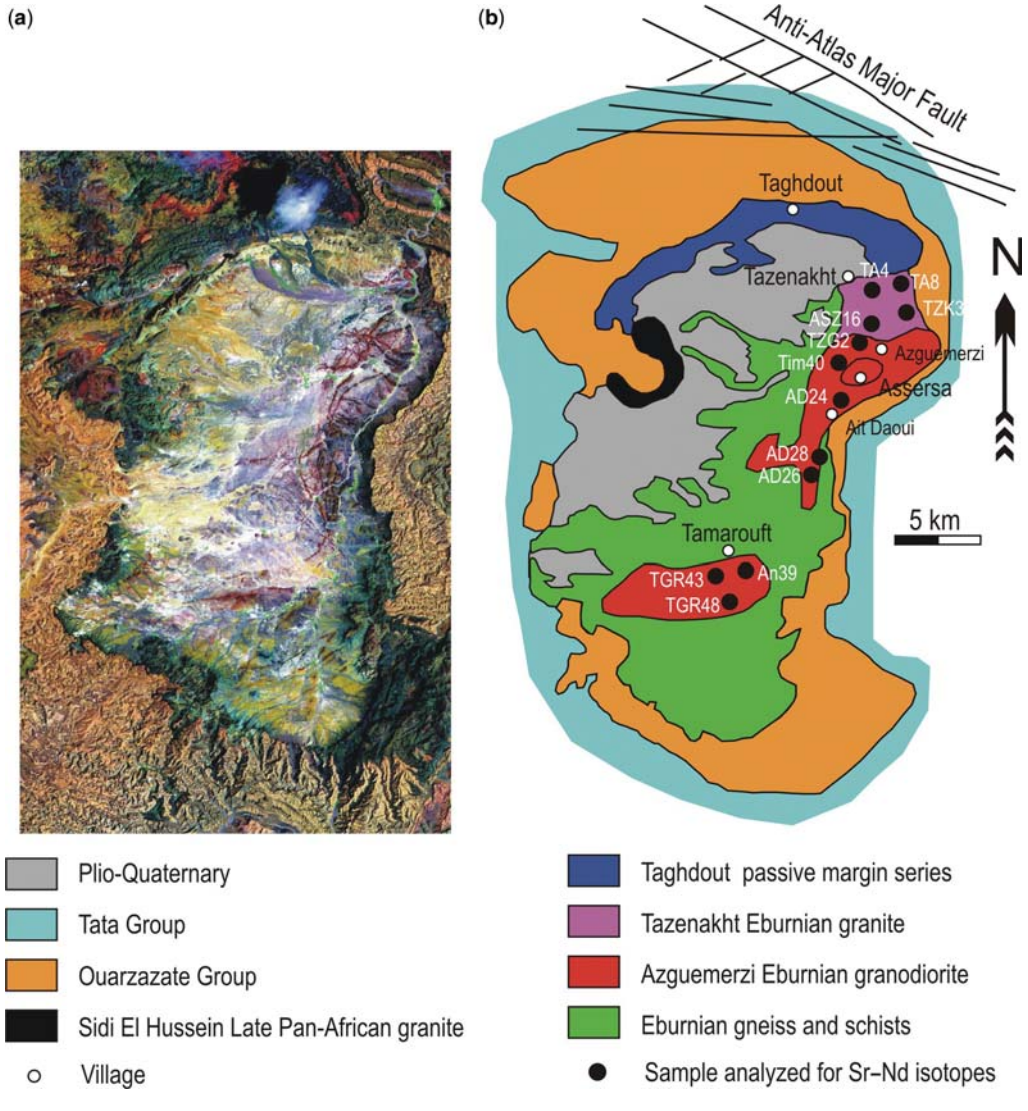

Fig. 3. (**a**) Satellite photograph of the Palaeoproterozoic Zenaga inlier (Orthorectified Landsat Thematic Mapper Mosaics as compressed colour imagery in MrSIDTM file format from Lizardtech). The inlier is noted 'Zenaga' on Figure 2a and 2b. (**b**) Sketch geological map of the Zenaga inlier (from Ennih & Liégeois 2001). The scales of the satellite image and of the geological map are the same.

dated at 761 ± 2 Ma and 762 ± 2 Ma at Taswirine (Sirwa area; U–Pb zircon; Samson *et al.* 2004) and a tonalitic migmatite at 743 ± 14 Ma at Iriri (Sirwa area; U–Pb zircon; Thomas *et al.* 2002). The zircon rims of the latter gave an age of 663 ± 13 Ma, interpreted as the age of the metamorphism that accompanied the island arc accretion towards the craton (Thomas *et al.* 2002). In Bou Azzer, juvenile metagabbros (752 ± 2 Ma), augen granite gneiss (753 ± 2 Ma) and leucogranites (705 ± 3 Ma; 701 ± 2 Ma) are linked to this 750–700 Ma event but in a way still to be deciphered (D'Lemos *et al.* 2006).

The Zenaga basement is overthrust by the Tamwirine rhyolitic unit, attributed to the Bou Salda Group, which has been dated at 605 ± 9 Ma (U–Pb zircon, Thomas *et al.* 2002). The Tamwirine rhyolites are unconformably overlain by the Ouarzazate Group. Rhyolites and granitoids of the Ouarzazate Group have been dated between 581 ± 11 Ma and 543 ± 9 Ma (Gasquet *et al.* 2005). Within the Zenaga inlier, the Sidi El Houssein alkaline

Table 1. *Major element compositions of Palaeoproterozoic Zenaga plutons*

Sample	SiO_2	TiO_2	Al_2O_3	Fe_2O_{3t}	MgO	MnO	CaO	Na_2O	K_2O	P_2O_5	LOS	SUM
Azguemerzi granodiorite												
TZG2	63.80	0.77	15.90	7.00	2.00	0.06	2.60	2.94	3.04	0.13	1.27	99.50
ASZ16	65.30	0.54	17.60	3.80	1.18	0.03	2.31	2.50	4.64	0.17	1.50	99.57
Tim40	66.00	0.53	16.50	4.17	1.54	0.03	2.57	2.42	3.94	0.17	1.87	99.74
Asra12	61.50	0.19	15.60	7.03	2.11	0.06	2.42	2.99	2.37	0.19	4.77	99.22
TGZ7	63.10	0.55	19.00	6.10	1.54	0.03	0.77	2.57	3.42	0.09	2.52	99.69
TT58	63.30	0.73	17.50	5.65	2.39	0.05	2.40	2.58	2.68	0.24	2.17	99.69
TL52	63.70	0.73	17.10	5.22	2.04	0.04	2.64	2.38	4.09	0.29	1.29	99.52
TL49	66.00	0.59	17.00	3.99	1.80	0.04	2.24	2.62	3.56	0.17	1.62	99.63
TL47	66.50	0.24	17.90	2.73	1.44	0.04	1.16	5.81	2.12	0.10	1.94	99.98
Tiz42	67.20	0.53	15.90	4.18	1.21	0.03	2.83	2.81	3.22	0.28	1.45	99.64
Ti31	67.90	0.33	16.50	2.56	0.81	0.03	1.83	2.70	4.79	0.20	1.96	99.61
TT21	68.00	0.51	15.90	4.93	1.80	0.09	0.25	2.26	3.58	0.09	2.45	99.86
TZG6	68.10	0.46	15.70	3.92	0.90	0.03	2.48	3.26	3.28	0.33	1.25	99.71
Tiz46	69.00	0.47	14.70	4.51	1.06	0.02	2.50	2.58	3.96	0.19	0.77	99.76
Tiz43	69.20	0.42	15.50	3.44	1.25	0.02	1.34	2.60	4.56	0.15	1.27	99.75
Ti30	69.70	0.26	16.90	2.24	0.49	0.01	0.35	2.51	6.10	0.13	1.15	99.84
Ti34	71.50	0.16	14.40	1.45	0.56	0.02	1.90	1.73	5.99	0.11	2.02	99.84
Ait Daoui monzogranite												
AD24	67.40	0.47	16.30	3.46	1.62	0.02	0.35	2.34	5.89	0.12	1.69	99.66
AD26	67.60	0.28	16.80	2.59	1.53	0.00	0.81	2.79	5.76	0.15	1.47	99.78
AD28	70.80	0.28	15.40	2.54	0.68	0.02	2.37	2.75	3.76	0.21	1.03	99.83
AD25	70.50	0.29	15.20	2.29	1.38	0.02	0.62	2.50	5.37	0.10	1.52	99.78
Assersa monzogranite												
Asra9	72.20	0.04	16.10	1.25	0.25	0.08	0.47	3.53	5.17	0.10	0.84	100.03
Asra11	74.70	0.01	14.20	0.91	0.11	0.01	0.66	3.28	5.46	0.18	0.44	99.96
As112	74.40	0.07	15.00	1.00	0.25	0.01	0.51	2.81	6.22	0.10	0.59	100.96
Asra10	73.40	0.01	15.30	4.98	0.10	0.02	0.55	4.04	4.04	0.12	0.47	103.02
As111	73.00	0.04	15.10	1.08	0.30	0.01	0.69	2.80	6.15	0.17	0.59	99.93
As114	71.90	0.47	14.80	3.45	1.19	0.02	1.28	2.44	2.64	0.10	1.51	99.80
Tamarouft monzogranite												
AN39	74.20	0.04	14.40	0.62	0.15	0.01	0.35	2.94	6.32	0.17	0.55	99.75
TGR43	70.60	0.03	18.10	1.31	0.48	0.01	0.47	3.50	3.68	0.32	1.44	99.93
TGR48	72.40	0.02	16.30	0.33	0.21	0.01	0.42	3.81	4.79	0.33	0.89	99.51
TAM31	66.30	0.54	15.70	5.24	2.23	0.03	1.37	4.67	2.47	0.20	1.11	99.86
TAM32	72.50	0.25	14.20	2.39	1.18	0.01	1.53	5.59	1.26	0.20	0.75	99.87
TAM33	71.50	0.02	16.10	0.96	0.27	0.01	0.75	2.94	5.58	0.30	1.42	99.84
TAM35	69.50	0.22	20.20	1.06	0.23	0.01	0.34	1.07	5.20	0.30	1.86	99.98
TOU37	71.10	0.28	15.50	2.41	0.44	93.00	0.53	3.46	4.91	0.11	1.05	192.79
TOU38	72.80	0.04	15.40	0.57	0.18	0.01	0.50	3.71	5.45	0.20	0.89	99.75
AN40	73.30	0.14	17.10	1.59	0.55	0.01	0.13	0.88	4.80	0.09	2.12	100.70
AN41	71.30	0.12	16.00	1.54	0.43	0.01	0.34	3.12	5.65	0.20	1.11	99.81
AN42	68.30	0.12	18.50	0.53	0.51	0.01	0.47	2.23	5.62	0.53	1.72	98.53
TGR44	71.20	0.00	16.10	0.22	0.07	0.00	0.20	2.53	8.87	0.31	0.36	99.86
TGR45	71.60	0.03	17.40	0.90	0.22	0.01	0.74	5.00	2.63	0.48	0.97	99.97
TGR46	71.10	0.02	17.10	0.73	0.17	0.01	0.40	4.42	4.21	0.31	0.87	99.33
TGR47	72.90	0.07	15.60	0.85	0.20	0.00	0.59	3.84	4.75	0.22	0.86	99.89
TAM44	70.10	0.32	16.90	1.11	0.42	0.01	0.85	2.87	5.70	0.49	1.25	100.01
Tazenakht monzogranite												
TZK3	73.00	0.07	14.80	0.85	0.25	0.01	0.40	2.00	7.53	0.17	0.75	99.84
TA4	73.10	0.15	14.70	1.55	0.07	0.00	0.45	3.88	5.34	0.03	0.51	99.77
TA8	75.10	0.02	15.50	0.70	0.19	0.01	0.51	5.22	1.72	0.27	0.83	100.07
Ti38	71.70	0.14	16.20	1.06	0.28	0.01	0.53	2.91	6.12	0.20	0.80	99.95
TZi101	72.85	0.10	15.44	1.11	0.35	0.01	0.38	3.73	4.80	0.16	1.07	100.00
TZi10B	72.88	0.10	15.38	1.23	0.34	0.01	0.41	3.83	4.69	0.19	0.96	100.02
TZi300	72.26	0.10	15.79	1.16	0.37	0.01	0.30	3.20	5.53	0.16	1.13	100.01
TZi500	73.02	0.09	15.29	1.13	0.34	0.01	0.26	3.01	5.50	0.16	1.20	100.01
TZi800	68.00	0.20	19.45	1.36	0.61	0.01	0.33	3.35	4.70	0.12	1.87	100.00
TZi100	73.28	0.12	15.27	1.10	0.33	0.01	0.32	3.49	4.82	0.18	1.07	99.99
TL51	70.00	0.12	17.00	0.80	0.27	0.00	0.43	2.76	7.08	0.14	1.29	99.89
AK18	72.30	0.24	14.90	1.94	0.42	0.01	0.66	3.45	4.69	0.12	0.99	99.72

Table 2. *Trace element compositions of Palaeoproterozoic Zenaga plutons*

Sample	V	Rb	Y	Zr	Nb	Ba	La	Ce	Pr	Nd	Sm	Eu
Azguemerzi granodiorite												
TZG2	44.2	98.8	32.8	228.4	8.3	958	50.0	105.6	12.24	47.0	8.44	1.45
ASZ16	21.4	89.0	15.0	196.8	7.1	1539	47.4	96.2	11.04	42.2	6.56	1.33
Tim40	25.1	92.6	11.8	165.8	7.2	812	35.0	74.1	8.76	33.1	6.14	1.03
Ait Daoui monzogranite												
AD26	26.6	153.9	15.1	167.8	8.9	1628	8.20	20.1	2.38	9.73	2.53	0.78
AD28	10.0	130.3	15.7	122.3	4.7	894	1.84	5.11	1.04	6.64	3.42	0.55
AD25	13.4	87.8	14.7	219.6	4.1	773	41.8	87.2	10.30	39.4	6.89	0.98
Assersa monzogranite												
Asra11	0.76	152.3	6.6	37.0	1.7	51	5.13	12.74	1.60	6.31	2.19	0.07
As112	0.44	121.5	12.5	26.9	0.8	79	7.00	14.38	1.78	6.90	2.31	0.06
Asra10	1.07	178.3	10.3	45.8	4.3	65	4.07	9.46	1.22	4.70	1.62	0.13
Tamarouft monzogranite												
TGR43	3.30	135.6	2.0	4.0	0.7	891	2.27	4.32	0.51	1.97	0.28	0.71
TGR48	<0.1	166.2	5.6	35.2	5.9	89	1.32	2.70	0.42	1.92	0.90	0.10
TAM31	<0.1	131.4	1.9	27.7	2.4	141	1.97	4.11	0.51	1.79	0.57	0.11
Tazenakht monzogranite												
TA4	1.21	157.1	26.1	42.9	1.4	841	19.16	39.2	4.76	17.7	3.97	0.75
TA8	3.86	135.3	39.4	198.5	9.6	867	36.0	76.5	9.00	35.2	7.13	0.74
Ti38	0.93	67.7	4.8	16.5	2.9	27	4.98	8.68	0.95	3.24	0.81	0.26

granitic ring-complex (579 ± 7 Ma; U–Pb zircon; Thomas *et al.* 2002) is contemporaneous with the Ouarzazate Group.

Structurally, the *c*. 2 Ga Eburnian deformation was high-grade and north–south to NE–SW orientated (Ennih *et al.* 2001). The Pan-African deformation occurred under greenschist conditions and is mostly NW–SE oriented along the AAMF corridor (Ennih *et al.* 2001). The Anti-Atlas was later deformed during the Late Palaeozoic Variscan orogeny, which was responsible for the generation of domes and for major décollements between the Palaeoproterozoic basement and the Neoproterozoic/Phanerozoic cover. Variscan deformation produced spectacular disharmonic folds in the Ouarzazate and Tata Groups and listric extensional faults within the basement (Faik *et al.* 2001; Burkhard *et al.* 2006), reactivating faults generated at the end of the Pan-African orogeny (Soulaimani *et al.* 2004). Those extensional structures were again reactivated during the Cenozoic Alpine orogeny generating the current relief of the Anti-Atlas with its Precambrian inliers and Cenozoic volcanism (**Berger *et al.***). Within the Palaeoproterozoic basement, attributing a structure to the Pan-African, Variscan or to the Alpine events is not easy because of the strong rheological contrast between the rigid basement and the softer sedimentary cover, inducing partition of the deformation. Even the rare thrust faults in the Zenaga basement that are generally interpreted as Pan-African in age could be Variscan or even Alpine in age (Thomas *et al.* 2002). However, it seems that the Variscan and Alpine events never induced thermal effects above 300 °C, based on the 580–525 Ma biotite-whole-rock mineral Rb–Sr dates obtained (Thomas *et al.* 2002).

The deformed Eburnian Zenaga granitoids are strongly peraluminous in character.

Analytical techniques

Whole-rock major and trace elements. Major elements have been measured by X-ray fluorescence (Université Catholique de Louvain) and the trace elements by ICP-MS (VG PQ2+, Royal Museum for Central Africa). For trace elements, the result of the alkaline fusion (0.3 g of sample + 0.9 g of lithium metaborate at 1000 °C during one hour) has been dissolved in 5% HNO_3. The calibrations were set using both synthetic solution (mixture of the considered elements at 2, 5 and 10 ppb) and international rock standards (BHVO-1, W1, GA, ACE). For all these elements, the precision varies from 5 to 10% (for details, see Navez 1995). Results are given in Table 1 (major elements) and Table 2 (trace elements).

Sr–Nd isotopes. After acid dissolution of the sample in a beaker or in a pressure vessel if any solid is present after centrifugation and Sr and Nd separation on ion-exchange resin, Sr isotopic compositions have been measured on Ta simple filament (VG Sector 54), Nd isotopic compositions on triple Ta–Re–Ta filament (VG Sector 54) in the Section of Isotope Geology of the Africa Museum,

Gd	Dy	Ho	Er	Yb	Lu	Hf	Ta	W	Pb	Th	U
6.45	5.73	1.31	3.54	3.64	0.55	6.85	0.28	0.77	20.3	14.1	1.48
4.63	3.10	0.64	1.41	1.32	0.21	6.04	0.26	0.70	18.2	11.0	0.84
4.48	2.59	0.47	1.05	0.94	0.14	5.16	0.35	1.15	16.2	11.1	1.03
3.19	3.16	0.67	1.76	1.65	0.23	5.22	0.31	0.57	21.7	21.1	1.74
3.97	3.11	0.63	1.60	1.36	0.19	3.94		0.37	22.6	10.0	1.35
4.65	3.04	0.59	1.33	1.15	0.17	7.01	0.20	0.57	20.7	11.3	1.29
2.28	1.73	0.25	0.42	0.26	0.04	1.90	0.06	1.04	17.1	3.04	1.58
2.97	2.93	0.37	0.49	0.16	0.02	1.54	0.03	1.13	19.1	2.52	1.57
1.92	2.03	0.36	0.71	0.52	0.06	2.17	0.04	0.37	24.8	2.70	1.19
0.62	0.73	0.15	0.41	0.37	0.06	0.14	0.10	0.85	26.0	0.85	0.49
1.15	1.38	0.24	0.64	0.96	0.14	1.60	0.80	2.30	1.7	0.88	1.20
0.71	0.89	0.17	0.41	0.48	0.08	1.29	0.23	1.42	9.2	0.82	1.97
4.24	4.47	0.85	2.00	1.55	0.22	1.57	0.15	0.57	32.2	5.09	2.67
7.28	7.06	1.54	4.17	4.20	0.62	7.02	0.75	1.16	11.3	13.9	2.40
0.92	1.23	0.26	0.76	0.95	0.15	0.64	0.51	1.27	2.8	0.44	0.43

Tervuren. Repeated measurements of Sr and Nd standards have shown that between-run error is better than 0.000015 (2σ). The NBS987 standard has given a value for $^{87}Sr/^{86}Sr$ of 0.710275 ± 0.000006 (2σ on the mean of 12 standards, normalized to $^{86}Sr/^{88}Sr = 0.1194$) and the Rennes Nd standard a value for $^{143}Nd/^{144}Nd$ of 0.511959 ± 0.000006 (2σ on the mean of 24 standards, normalized to $^{146}Nd/^{144}Nd = 0.7219$) during the course of this study. All measured ratios have been normalized to the recommended values of 0.710250 for NBS987 and 0.511963 for Nd Rennes standard (corresponding to a La Jolla value of 0.511858) based on the 4 standards measured on each turret together with 16 samples. Decay constant for ^{87}Rb (1.42×10^{-11} a^{-1}) was taken from Steiger & Jäger (1977) and for ^{147}Sm (6.54×10^{-12} a^{-1}) from Lugmair & Marti (1978). Results are given in Table 3.

Geology and petrography

The Azguemerzi porphyritic biotite-granite is a coarse-grained, zoned and mesocratic rock. The primary minerals are mainly plagioclase and mega-alkali feldspar which are resorbed and largely sericitized. The mega-alkali feldspar occurs as coarse perthitic orthoclase megacrysts and medium grained microcline. Myrmekitic intergrowths are uncommon, but when present, pervasive and large orthoclase megacrysts are occasionally surrounded by a composite mantle of plagioclase and quartz. The quartz is typically interstitial and forms late stage inclusions. The main mafic magmatic silicates are biotite, garnet and the epidote, which is included in or associated with biotite (most of the epidote is secondary). Accessory minerals include anhedral, rounded zoned zircon, euhedral apatite, titanite, and ilmenite. Secondary minerals are sericite, chlorite and most of the epidote. The Azguemerzi pluton shows quartzo-feldspathic layers separated by biotite layers, locally associated with gneisses and anatectites in the Assersa and in Tizi-n-Taguergoust valleys. The Azguemerzi pluton displays a magmatic fabric which evolves locally to a true foliation, which probably explains why it was sometimes regarded as porphyritic gneiss. It contains xenolithic micaschists and gneisses of metasedimentary nature which could represent the source of these rocks but are most probably xenoliths from the country-rocks.

The Assersa, Aït Daoui and Tamarouft are granodiorite and monzogranite plutons that show the same mineralogical assemblage as the Azguemerzi pluton without biotite, conferring their leucocratic character. The Tazenakht granite in the northern part of Zenaga is a heterogeneous coarse-grained rock. It consists of abundant euhedral alkali feldspar phenocrysts, xenomorphic crystals of quartz, subhedral sericitized polycrystalline plagioclase, twisted biotite and sometimes twisted muscovite. Decimetre-size pegmatitic pockets are associated with acidic pegmatitic and aplopegmatitic dykes. Accessory minerals are mainly oxides; rare corundum has been observed. This granite was generally

Table 3. *Sr and Nd isotopes of Palaeoproterozoic Zenaga plutons*

Pluton	Sample	Rb	Sr	$^{87}Rb/^{86}Sr$	$^{87}Sr/^{86}Sr$	2σ	Sri 600 Ma	Sri 2035 Ma	Sm
Azguemerzi	TZG2	110	172	1.858	0.749223	0.000012	0.733323	0.694741	8.44
Azguemerzi	ASZ16	92	185	1.444	0.741828	0.000009	0.729473	0.699494	6.56
Azguemerzi	Tim40	95	140	1.975	0.766482	0.000014	0.749583	0.708577	6.14
Assersa	Asra9	165	16	32.291	1.539725	0.000015	1.263430	0.592997	2.19
Assersa	Asra11	140	17	24.876	1.152029	0.000015	0.939183	0.422712	2.31
Assersa	As112	178	21	26.443	1.499209	0.000015	1.272951	0.723935	1.62
Aït Daoui	AD 24	162	116	4.074	0.790233	0.000008	0.755372	0.670782	2.53
Aït Daoui	AD 26	150	156	2.798	0.764744	0.000009	0.740802	0.682706	3.42
Aït Daoui	AD 28	90	138	1.895	0.749736	0.000007	0.733521	0.694175	6.89
Tamarouft	An39	143	170	2.449	0.768874	0.000008	0.747920	0.697076	0.28
Tamarouft	TGR43	193	14	42.804	1.447583	0.000017	1.081334	0.192629	0.90
Tamarouft	TGR48	155	29	15.974	1.039992	0.000012	0.903314	0.571665	0.57
Tazenakht	TZK3	159	135	3.437	0.792343	0.000011	0.762937	0.691584	3.97
Tazenakht	TA4	135	34	11.576	0.783725	0.000011	0.684674	0.444326	7.13
Tazenakht	TA8	68	63	3.155	0.809272	0.000008	0.782279	0.716779	0.81

T_{DM} model ages calculated following Nelson & DePaolo (1985). For altered samples, the magmatic ϵ_{Nd} and the T_{DM} model ages have been calculated, using the $^{147}Sm/^{144}Nd$ ratio from 600 to 2035 Ma, of an unaltered sample, from the same pluton (column '$^{147}Sm/^{144}Nd$ used').

deformed in a solid state; it has a planar structure formed with mega-alkali feldspar sometimes fractured, twisted and kinked muscovite and biotite with heterogeneous levels corresponding to mylonitic rocks. Towards the south, the mega-alkali feldspars are deformed within a very intense foliation near the contact of the Azguemerzi granite. These characters reflect an intense and heterogeneous deformation, locally transforming the Tazenakht granite into orthogneiss, porphyroblastic mylonites and phyllonitic layers.

A main characteristic of the Zenaga granitoids is the abundant presence of peraluminous minerals with abundant muscovite and almandine-rich garnet ($Alm_{71\text{-}89}$ $Pyr_{3\text{-}14}$ $Sps_{2\text{-}12}$), except the Tazenakht granite which does not bear garnet but is particularly rich in muscovite and locally contains corundum.

Major elements

The studied Palaeoproterozoic granitoids (location in Fig. 3b) are all mainly felsic ($SiO_2 > 68\%$) except the Azguemerzi granodiorite, which is intermediate in composition (most samples are in the range 61–70% SiO_2). They have variable compositions in alkalis and straddle the boundaries defined for the alkalic, alkali-calcic, calc-alkalic and calcic series (Fig. 4a) suggesting a heterogeneous source or some alkali mobility. They are always strongly peraluminous (Fig. 4b) and yield an alumina saturation index (ASI) decreasing with silica, which points to a peraluminous melt crystallizing aluminous minerals. The Al_2O_3 activity in the melts compared with the ASI (Patiño-Douce 1992) shows that the Zenaga granitoids are chemically comparable to other garnet bearing granitoids (Fig. 4c) pointing to a heterogeneous peraluminous source rather than to alkali mobility.

This high peraluminosity indicates the presence in the source of a strongly peraluminous component, i.e. a pelitic continental crust, with, considering the quite high Ca, Na, Mg and Fe concentrations in these granitoids, the addition of a basaltic component. The garnet can crystallize from the melt itself (Dahlquist *et al.* 2007) or from the incongruent melting of a muscovite + biotite + quartz assemblage in the pelitic source that gives melt and garnet at *c.* 650 °C. In all cases, a muscovite-rich source is needed, the only mineral that undergoes substantial dehydration at temperature <800 °C (Miller *et al.* 2003).

REE and Nd isotopes as markers of the Pan-African metacratonic evolution of the Zenaga Eburnian basement

The rare earth element (REE) patterns of the five plutons studied display very varied shapes considering that all rocks are within the 64–75% SiO_2 range. The Azguemerzi granodiorites display normal REE patterns for granodiorite, except the large variability in HREE abundance that can be attributed to variable garnet control (Fig. 5a). The Tazenakht granite (Fig. 5b) has one sample (TA8) very low in REE and with no Eu negative anomaly, which is very different from the two

Nd	$^{147}Sm/^{144}Nd$	$^{143}Nd/^{144}Nd$	2σ	ε_{Nd} 600 Ma	ε_{Nd} 2035 Ma	Magmatic ε_{Nd} (see text) $^{147}Sm/^{144}Nd$ used	2035 Ma	T_{DM} (Ma)
47.00	0.1085	0.511472	0.000009	−16.01	0.30	measured	0.38	2284
42.22	0.0939	0.511356	0.000006	−17.15	1.86	measured	1.93	2151
33.14	0.1121	0.511546	0.000007	−14.84	0.81	measured	0.89	2253
6.31	0.2104	0.512862	0.000008	3.32	0.79	measured	0.94	
6.90	0.2026	0.512699	0.000007	0.74	−0.36	measured	−0.22	
4.70	0.2084	0.512539	0.000008	−2.84	−5.03	0.18 (estimated)	0.38	
9.73	0.1573	0.511747	0.000008	−14.38	−7.12	0.1058 = AD28	2.52	2120
6.64	0.3117	0.512344	0.000007	−14.58	−35.99	0.1058 = AD28	2.32	2135
39.40	0.1058	0.511510	0.000011	−15.05	1.77	0.1058 (measured)	1.84	2170
1.97	0.0843	0.511967	0.000032	−4.47	16.37	0.1911 = TGR48	−3.32	
1.92	0.2833	0.512959	0.000009	−0.38	−16.45	0.1911 = TGR48	0.79	
1.79	0.1911	0.512524	0.000011	−1.80	−0.77	0.1911 (measured)	−0.63	
17.70	0.1357	0.511978	0.000014	−8.21	3.07	0.1357 (measured)	3.17	2086
35.24	0.1223	0.511972	0.000007	−7.30	6.49	0.1357 = TZK3	4.09	1992
3.24	0.1520	0.511963	0.000010	−9.76	−1.50	0.1357 = TZK3	1.62	2245

other samples; the Eu abundance of sample TA4 is similar to that of sample TZK3 but its other REE are much higher, suggesting a possible beginning of tetrad effect (enrichment in REE due to F-rich fluids; Bau 1996; Veksler *et al.* 2005). The three samples from the Tamarouft pluton (Fig. 5c) display low abundance of REE, low REE fractionation and variable Eu anomaly. Sample TGR48 displays an REE pattern that could be magmatic; the two other samples show unusual spectra: sample TGR43 is richer in normalized HREE than in LREE and sample AN39 has a strong positive Eu anomaly and also higher normalized HREE than LREE. The three samples from the Ait Daoui pluton (Fig. 5d) have similar HREE but very dissimilar LREE. Sample AD28 has a normal magmatic pattern whereas sample AD26 suffered a strong loss in LREE and sample AD24 has nearly no Eu anomaly and a weak LREE/HREE fractionation. The three samples from the Assersa granite (Fig. 5e) display from La to Eu spectra similar to seagull patterns but a strong depletion in HREE. This suggests the influence of F-rich fluids (for the tetrad effect) coupled to the destabilization of a HREE-rich mineral such as garnet, present in this granite.

All these REE patterns indicate that some Zenaga granitoids possess normal REE patterns whereas others do not; the latter suggest an important role for fluids, probably enriched in elements such as F (Veksler *et al.* 2005). Such fluids are not typical in strongly peraluminous magmas, except for extremely differentiated melts, which is not the case in Zenaga. They are much more similar to the characteristics of alkaline magmas, frequently displaying seagull REE spectra (Bau *et al.* 1996). This leads to the question of the age of the fluid influence: these could be late-magmatic fluids or much younger fluids derived by reactivation of the northern boundary of the WAC. The use of the Nd isotopes can constrain this topic.

Initial $^{143}Nd/^{144}Nd$ values relative to bulk Earth (ε_{Nd}) are highly variable in the studied plutons: they vary from −36 to +16. This variation is observed within all the plutons studied, although the most extreme values belong to the Tamarouft and Ait Daoui plutons (Table 3).

When looking closely at the evolution of the ε_{Nd} through time for the different plutons (Fig. 6), several observations emerge. The Azguemerzi granodiorite (Fig. 6a) displays the expected evolution for a magmatic rock: similar slope (proportional to the $^{147}Sm/^{144}Nd$ ratio), grouped ε_{Nd} at 2035 Ma (U–Pb zircon crystallization age), and a progressively larger variability of ε_{Nd} while time is elapsing (common ε_{Nd} at 2035 Ma, slight difference in $^{147}Sm/^{144}Nd$ ratios between samples inducing progressive difference in the produced radiogenic ^{143}Nd). The Tazenakht granite (Fig. 6b) shows the opposite behaviour: ε_{Nd} are distinct at 2035 Ma and become more and more similar with time. The Tamarouft and Ait Daoui plutons (Fig. 6c, 6d) display crossed patterns: ε_{Nd} are very different at 0 Ma and 2035 Ma, having a common value during the Neoproterozoic. Finally, the Assersa pluton (Fig. 6e) shows parallel evolution, the difference in ε_{Nd} of the three samples remaining nearly constant through time.

The spectra of the Tamarouft and Ait Daoui plutons are particularly enlightening: their ε_{Nd}

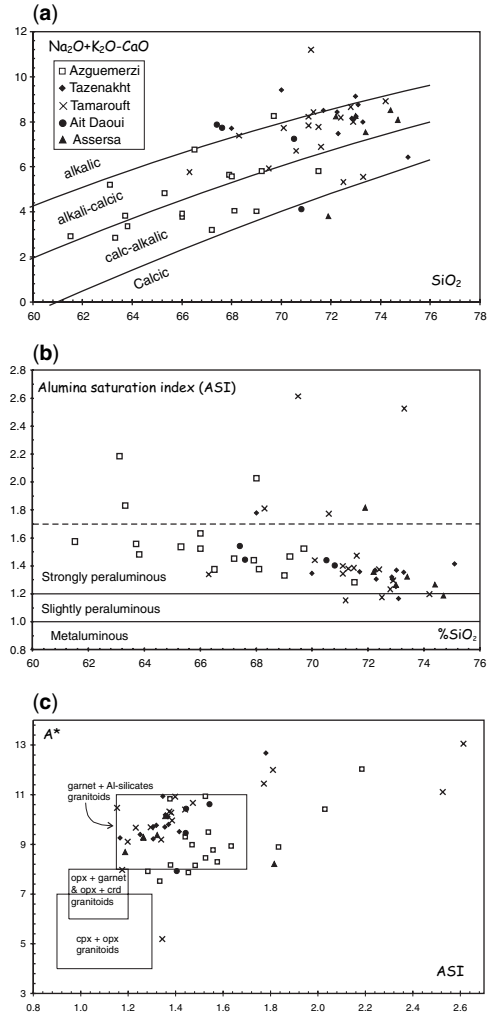

Fig. 4. (**a**) SiO_2 *vs.* $Na_2O + K_2O$-CaO (MALI index; Frost *et al.* 2001). (**b**) Alumina saturation index (ASI) = $Al_2O_3/(Na_2O + K_2O + CaO)$ in molar proportions *vs.* SiO_2 showing the strong peraluminous character of the Palaeoproterozoic Zenaga granitoids. (**c**) A* (=ASI *$(Na_2O + K_2O)$) *vs.* ASI (Patiño-Douce 1992); boxes for the three kind of peraluminous granitoids are based to the analyses compiled by Patiño-Douce (1992).

values are very close to ages corresponding to the Pan-African orogeny. Three-point isochrons can even be calculated: the Ait Daoui gives an age of 612 ± 300 Ma (initial $^{143}Nd/^{144}Nd = 0.51110 \pm 0.00040$; MSWD = 8.5) and Tamarouft an age of 761 ± 300 Ma (initial $^{143}Nd/^{144}Nd = 0.51156 \pm 0.00041$; MSWD = 2.4). These ages are imprecise but they strongly suggest that, during the Pan-African, the REE of some studied samples were remobilized, as indicated by both $^{143}Nd/^{144}Nd$ isotopic ratios and REE abundances. Such a remobilization requires aggressive F-rich fluid percolations. The hydrothermal event can be linked to the Ouarzazate Supergroup that crosscuts and covers the Zenaga inlier: this is a huge volcanic episode, alkali-calcic in nature and associated with fluorine and beryl that has formerly been mined. This hypothesis can be tested by using an evolutionary model in two stages, with the measured $^{147}Sm/^{144}Nd$ ratios of the sample from now to 600 Ma (Pan-African orogeny) and with the magmatic $^{147}Sm/^{144}Nd$ ratio that can be estimated from unaltered samples from 600 to 2035 Ma (U–Pb on zircon crystallization age). The Variscan and Alpine events are not considered here for two reasons: (1) the above mentioned convergence of ε_{Nd} occurred during the Pan-African and (2) the two Phanerozoic events happened at temperature $< 300^{\circ}C$ in the Zenaga inlier (Thomas *et al.* 2002).

The unaltered Azguemerzi samples (Fig. 5a) can be taken as reference for the magmatic signature of the Eburnian Zenaga plutons: their ε_{Nd} at 2035 Ma vary between +0.3 and +1.9. In the Ait Daoui pluton, the AD28 sample has a magmatic REE pattern (Fig. 5d) and gives a ε_{Nd} of +1.8, within the Azguemerzi range. This sample can, therefore, be considered as having a REE magmatic signature. Its $^{147}Sm/^{144}Nd$ ratio can be used from 600 to 2035 Ma for the two other samples of the Ait Daoui pluton: with this two stage evolution, sample AD24 get a ε_{Nd} at 2035 Ma of +2.5 and sample AD26 a ε_{Nd} of +2.3 (Fig. 6d), very close to the Azguemerzi range. In a similar way, sample TGR48 from the Tamarouft pluton can be considered as having a magmatic REE signature (ε_{Nd} at 2035 Ma = −0.8) and when using its $^{147}Sm/^{144}Nd$ ratio from 600 to 2035 Ma (Fig. 6e), one of the other samples get an Azguemerzi-like εNd values (sample TGR43, ε_{Nd} at 2035 Ma = +0.8) and the other sample (AN39) get a lower εNd of −3.3 but however much more magmatic compatible that its single stage ε_{Nd} of +16.4 (Fig. 6d).

The Tazenakht TZK23 sample, which shows a classical magmatic REE pattern (Fig. 5b), has a ε_{Nd} at 2035 Ma of +3.1. With the TZK23 $^{147}Sm/^{144}Nd$ ratio, the two other samples provide ε_{Nd} at 2035 Ma of +1.6 and +4.1 (Fig. 6b). Finally, if the samples from the Assersa pluton have lost a part of their HREE content (Fig. 5e), a feature likely to be linked to the fact that the garnet in this pluton is altered to chlorite and epidote, their LREE values appear to be less affected. Their ε_{Nd} at 2035 Ma are +0.8 (Asra 9), −0.36 (Asra11) and −5.03 (As112). The first two are within the range of the Azguemerzi pluton. Sample As112 has a lower ε_{Nd} but this sample is

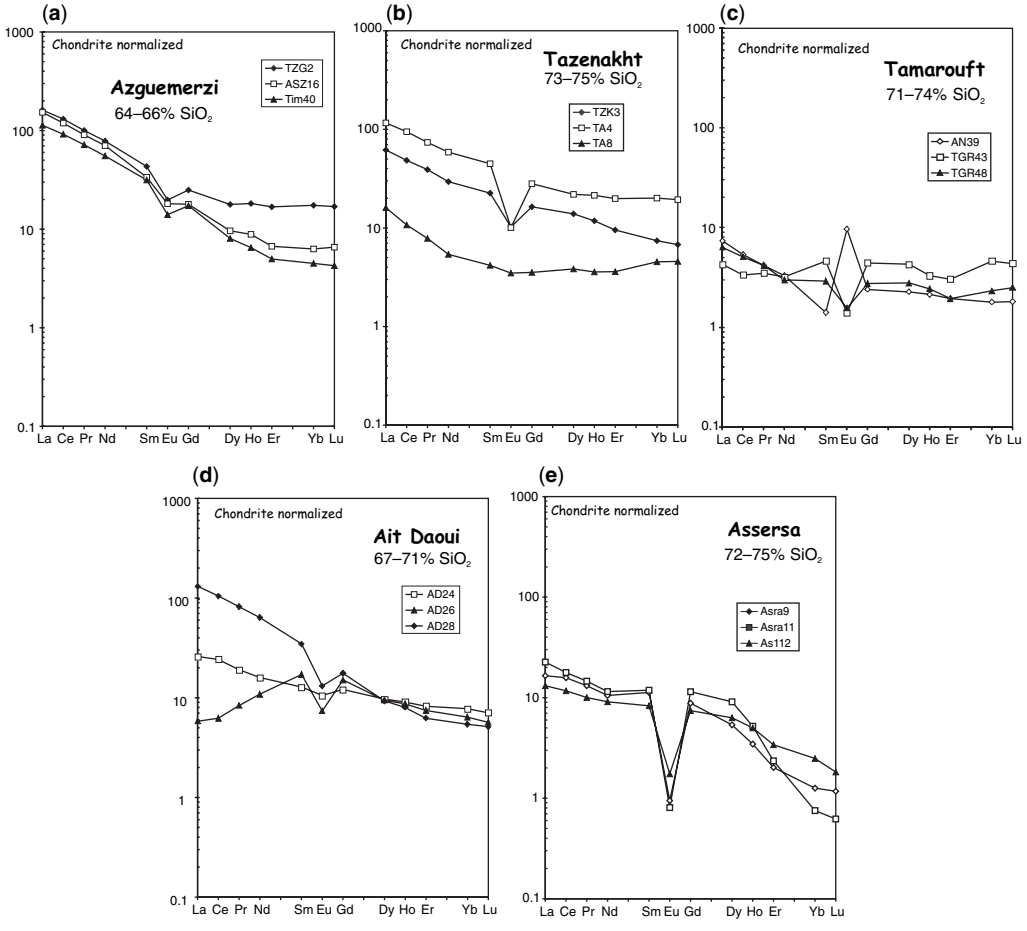

Fig. 5. Rare Earth Elements normalized to chondrites (Boynton 1984) for the studied Zenaga granitoids, showing the F-rich fluids influence on some of the samples. (**a**) Azguemerzi granodiorite; (**b**) Tazenakht granite; (**c**) Tamarouft granite; (**d**) Ait Daoui granite; (**e**) Assersa granite.

REE-poor and with a Sm concentration of 1.4 ppm (against the measured value of 1.6 ppm), this sample would have a ε_{Nd} at 2035 Ma of +0.38 (Fig. 6e).

These results show that, when using magmatic $^{147}Sm/^{144}Nd$ ratios deduced from pristine samples for all samples from 600 Ma to 2035 Ma, the obtained ε_{Nd} at 2035 Ma are quite homogeneous, varying from −0.8 to +2.5 for most samples, with one sample at −3.3 and two samples at +3.1 and +4.1 (Fig. 6f); with the recalculated values, the mean ε_{Nd} at 2035 Ma for the Zenaga plutons is remarkably determined at $+1.1 \pm 0.9$. This indicates a mainly juvenile source (ε_{Nd} of the depleted mantle at 2035 Ma = +5.5), which is also indicated by the T_{DM} model ages of the samples having $^{147}Sm/^{144}Nd < 0.15$ (measured or recalculated) whose mean is 2159 ± 61 Ma. The calculation for the other samples would have implied a three-stage evolution and would have given similar model ages. They denote that major REE fractionation existed in the source, which, coupled with the strongly peraluminous character of the Zenaga granitoids, is consistent with a metasedimentary juvenile continental crustal source combining metasedimentary formations and mafic rocks melted at depth. More details about the nature of the Eburnian orogeny in the Anti-Atlas require further constraints on the Zenaga metamorphic basement whose age, according to the inherited zircons dated in the granitoids, would be around 2.17 Ga (Thomas *et al.* 2002).

Sr isotopes have been largely modified by the Pan-African event: at 2035 Ma, most of the $^{87}Sr/^{86}Sr$ initial ratios are much lower than 0.7.

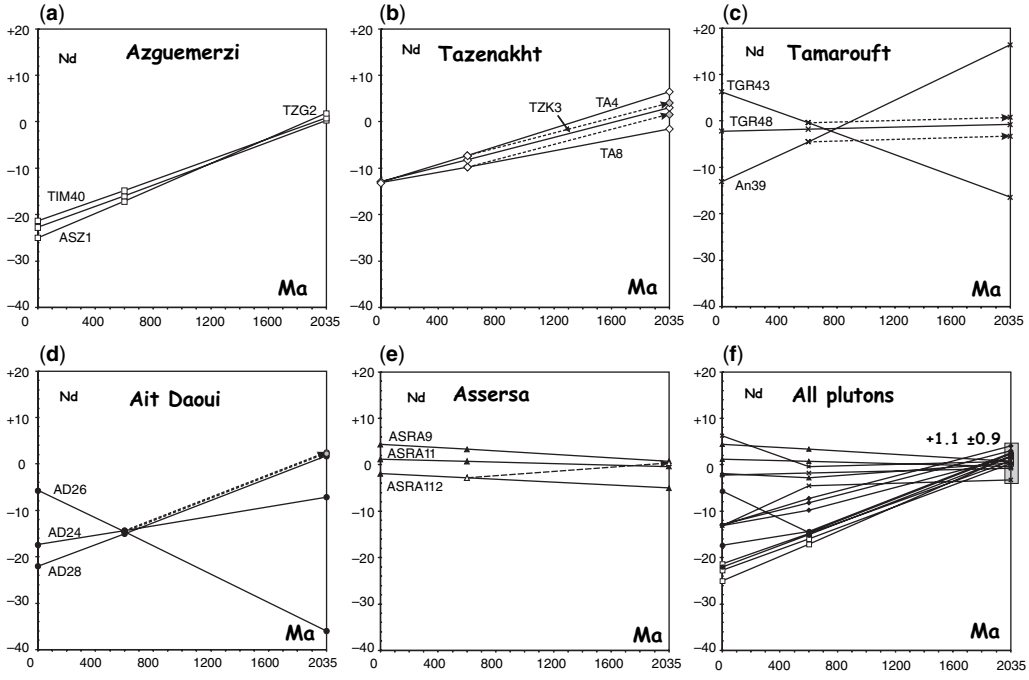

Fig. 6. Nd isotopes (shown as $\varepsilon_{Nd} = [(^{143}Nd/^{144}Nd)_{sample}-(^{143}Nd/^{144}Nd)_{Bulk\text{-}Earth}]/(^{143}Nd/^{144}Nd)_{Bulk\text{-}Earth}$, both sample and Bulk Earth Nd isotopic compositions being calculated at the time considered. Full lines are the evolution calculated with the measured $^{147}Sm/^{144}Nd$ ratio of the sample (single stage evolution). The dashed lines from 600 Ma (age of the Pan-African perturbation) to 2035 Ma (age of the granite crystallization; U–Pb zircon, Thomas *et al.* 2002) are the evolutions calculated with the $^{147}Sm/^{144}Nd$ ratio of unaltered samples during the Pan-African orogeny, from the same pluton (two-stage evolution). See text for more explanation. (**a**) Azguemerzi granodiorite; (**b**) Tazenakht granite; (**c**) Tamarouft granite; (**d**) Ait Daoui granite; (**e**) Assersa granite; (**f**) All plutons together with measured magmatic $^{147}Sm/^{144}Nd$ ratios (single stage evolution) or adopted $^{147}Sm/^{144}Nd$ ratios (two-stage evolution).

The alignment (with a poor MSWD of 190) determined by the 15 samples gives an 'age' of 1467 ± 310 Ma (initial $^{87}Sr/^{86}Sr = 0.711 \pm 0.078$). This 'age' is the result of the interplay of the Eburnian age of the granitoids and the major Pan-African effect.

Conclusions

The chemical and isotopic data for the Zenaga Palaeoproterozoic magmatism indicate that these peraluminous granitoids originated from the partial melting of a juvenile, largely metasedimentary, crustal source but that the Pan-African orogeny has strongly reactivated some plutons or parts of plutons, including REE. The likely cause was the circulation of F-rich fluids circulation linked to the extrusion of the voluminous Ouarzazate Group and the emplacement of associated plutons (*c.* 580 Ma) along reactivated faults and shear zones. The reactivation event occurred during important vertical movements (the thickness of the Ouarzazate Group varies from 0 to more than 2500 m) but without major crustal or lithospheric thickening. This is demonstrated by the low-grade character of the Pan-African metamorphism (greenschist facies) and by the excellent preservation of the *c.* 800 Ma passive margin sediments and the early *c.* 750–700 Ma ophiolitic complex. This is considered to be typical of a metacratonic evolution: the cratonic boundary was dissected by faults and invaded by magmas but preserved most of its rigidity and primary features. Such a metacratonic reactivation was favourable for fluid circulation, in this case able to mobilize rare-earth elements. Such fluid movements were also an excellent vector for element concentration and genesis of mineralizations, for which the Anti-Atlas is internationally renowned.

This book concerns an example of these areas of paramount importance that are the boundaries of craton that suffered partial reactivation, i.e. a metacratonic evolution. The West African craton is a particularly good example because: (1) it became a strong craton during the Mesoproterozoic, a

period of 600 Ma that left no trace on the WAC; (2) all its boundaries intervened as indentors during the Pan-African orogeny leading to situations varying from nearly frontal collision to nearly entirely transcurrent dockings; (3) only its western and northern boundaries were included as foreland in the Variscan collision, allowing fruitful comparison between the eastern and the western WAC boundaries; (4) the WAC boundaries were major suppliers of lithospheric pieces or of sedimentary material for the Peri-Gondwanan terranes now located in Europe or in North America; (5) currently, the WAC boundaries are reactivated by the stress generated by the Africa-Europe convergence and constitutes a key area for studying intraplate deformation submitted to stress; (6) WAC boundaries, or at least a part of them, are known for their mined or potential mineral deposits. A better knowledge of the boundaries of the West African craton is a prerequisite for understanding all these processes. This is the aim of the papers constituting this Special Publication.

This is a contribution to the IGCP485. We warmly thank the UNESCO and the IUGS for their financial support and encouragements during these five years. We are happy that this Special Publication comes out during the International Year of Planet Earth, an outstanding outcome from these two organizations. Organizing contacts and field meetings in the desert regions of Mauritania, Mali, Algeria and Morocco was always a challenge but also very stimulating. We would like to thank Khalidou Lô (Mauritania), Samba Sacko (deceased), Dramane Dembélé, Renaud Caby (Mali), Khadidja Ouzegane, Abla Azzouni-Sekkal (Algeria), Ezzoura Errami Hassan Admou, Hassan Ouanaimani, and Abdelilah Fekkak (Morocco) for their personal support and the support of organizations in their country. We are also grateful to the Universities of Algiers (USTHB) and El Jadida, the Office Mauritanien de Recherches Géologiques, the Direction Nationale de la Géologie et des Mines de Bamako, the Algerian COMENA as well as the Ministries of Mines and Energy of Mauritania, Mali and Algeria. We warmly thank Bernard Bonin for judicious remarks on key points of the paper and Kevin Hefferan for detailed and helpful remarks and corrections. Both have suggested significant improvements to this article. Finally, we would like to thank the Publication team of the Geological Society for their support and patience.

References

ABDELSALAM, M, LIÉGEOIS, J. P. & STERN, R. J. 2002. The Saharan metacraton. *Journal of African Earth Sciences*, **34**, 119–136.

ABOUCHAMI, W., BOHER, M., MICHARD, A. & ALBARÈDE, F. 1990. A major 2.1 Ga event of mafic magmatism in West Africa: an early stage of crustal accretion. *Journal Geophysical Research*, **95**, 17605–17629.

AFFATON, P., RAHAMAN, M. A., TROMPETTE, R. & SOUGY, J. 1991. The Dahomeyide Orogen: tectonothermal evolution and relationships with the Volta basin. *In*: DALLMEYER, R. D. & LECORCHÉ, J. P. (eds) *The West African Orogens and Circum-Atlantic Correlatives*. Springer, Berlin, 107–122.

AKO, J. A. & WELLMAN, P. 1985. The margin of the West African craton: the Voltaian basin. *Journal of the Geological Society, London*, **142**, 625–632.

AZZOUNI-SEKKAL, A., LIÉGEOIS, J. P., BECHIRI-BENMERZOUG, F., BELAIDI-ZINET, S. & BONIN, B. 2003. The 'Taourirt' magmatic province, a marker of the very end of the Pan-African orogeny in the Tuareg Shield: review of the available data and Sr-Nd isotope evidence. *Journal of African Earth Sciences*, **37**, 331–350.

BATES, R. L. & JACKSON, J. A. (eds) 1980. *Glossary of Geology*. American Geological Institute, Falls Church, Virginia.

BAU, M. 1996. Controls on the fractionation of isovalent trace elements in magmatic and aqueous systems. Evidence from Y/Ho, Zr/Hf and lanthanide tetrad effect. *Contributions to Mineralogy and Petrology*, **123**, 323–333.

BLACK, R. & LIÉGEOIS, J. P. 1993. Cratons, mobile belts, alkaline rocks and continental lithospheric mantle: the Pan-African testimony. *Journal of the Geological Society, London*, **150**, 89–98.

BLACK, R., CABY, R., MOUSSINE-POUCHKINE, A., BERTRAND, J. M. L., BOULLIER, A. M., FABRE, J. & LESQUER, A. 1979. Evidence for Precambrian plate tectonics in West Africa. *Nature*, **278**, 223–227.

BLACK, R., LATOUCHE, L., LIÉGEOIS, J. P., CABY, R. & BERTRAND, J. M. 1994. Pan-African displaced terranes in the Tuareg shield (central Sahara). *Geology*, **22**, 641–644.

BOHER, M., MICHARD, A., ALBARÈDE, F., ROSSI, M. & MILÉSI, J. P. 1992. Crustal growth in West Africa at 2.1 Ga. *Journal Geophysical Research*, **97**, 345–369.

BOUOUGRI, E. H. & SAQUAQUE, A. 2004. Lithostratigraphic framework and correlation of the Neoproterozoic northern West African craton passive margin sequence (Siroua, Zenaga, Bouazzer-Elgraara inliers, Central Anti-Atlas, Morocco): an integrated approach. *Journal of African Earth Sciences*, **39**, 227–238.

BOYTON, W. V. 1984. Geochemistry of the rare earth elements: meteorite studies. *In*: HENDERSON, P. (ed.) *Rare Earth Element Geochemistry*. Elsevier, 63–114.

BRONNER, G., ROUSSEL, J., TROMPETTE, R. & CLAUER, N. 1980. *Genesis and Geodynamic Evolution of the Taoudeni Cratonic Basin (Upper Precambrian and Paleozoic), Western Africa, Dynamics of Plate Interiors.* Geodynamics Series vol. 1, American Geophysical Union, 81–90.

BURKHARD, M., CARITG, S., HELG, U., ROBERT-CHARRUE, C. & SOULAIMANI, A. 2006. Tectonics of the Anti-Atlas of Morocco. *Comptes Rendus Geoscience*, **338**, 11–24.

CABY, R., ANDREOPOULOS-RENAUD, U. & PIN, C. 1989. Late Proterozoic arc-continent and continent-continent collision in the Pan-African trans-Saharan belt of Mali. *Canadian Journal of Earth Sciences*, **26**, 1136–1146.

CALVEZ, J. Y. & VIDAL, P. 1978. Two billion years old relicts in the Hercynian belt of Western Europe. *Contributions to Mineralogy and Petrology*, **65**, 395–399.

CARITG, S., BURKHARD, M., DUCOMMUN, R., HELG, U., KOPP, L. & SUE, C. 2004. Fold interference patterns in the Late Palaeozoic Anti-Atlas belt of Morocco. *Terra Nova*, **16**, 27–37.

DAHLQUIST, J. A., GALINDO, C., PANKHURST, R. J., RAPELA, C. W., ALASINO, P. H., SAAVEDRA, J. & FANNING, C. M. 2007. Magmatic evolution of the Peñón Rosado granite: Petrogenesis of garnet-bearing granitoids. *Lithos*, **95**, 177–207.

DECKART, K., BERTRAND, H. & LIÉGEOIS, J. P. 2005. Geochemistry and Sr, Nd, Pb isotopic composition of the Central Atlantic Magmatic Province (CAMP) in Guyana and Guinea. *Lithos*, **82**, 282–314.

DE LA BOISSE, H. 1979. Pétrologie et geochronologie des roches cristallophylliennes du bassin de Gourma (Mali), conséquences pétrogénétiques. Unpublished PhD thesis, Montpellier.

D'LEMOS, R. S., INGLIS, J. D. & SAMSON, S. D. 2006. A newly discovered orogenic event in Morocco: Neoproterozoic ages for supposed Eburnean basement of the Bou Azzer inlier, Anti-Atlas mountains. *Precambrian Research*, **147**, 65–76.

ENNIH, N. & LIÉGEOIS, J. P. 2001. The Moroccan Anti-Atlas: the West African craton passive margin with limited Pan-African activity. Implications for the northern limit of the craton. *Precambrian Research*, **112**, 291–304.

ENNIH, N., LADURON, D., GREILING, R. O., ERRAMI, E., DE WALL, H. & BOUTALEB, M. 2001. Superposition de la tectonique éburnéenne et panafricaine dans les granitoïdes de la bordure nord du craton ouest africain, boutonnière de Zenaga, Anti-Atlas central, Maroc. *Journal of African Earth Sciences*, **32**, 677–693.

FABRE, J. 2005. *Géologie du Sahara occidental et central*. Série/Reeks: Tervuren African Geosciences Collection, MRAC Tervuren, Belgique.

FAIK, F., BELFOUL, M. A., BOUABDELLI, M. & HASSENFORDER, B. 2001. Les structures de la couverture néoprotérozoïque terminal et paléozoïque de la région de Tata, Anti-Atlas centre-occidental, Maroc: déformation polyphasée, ou interactions socle/couverture pendant l'orogenèse hercynienne? *Journal of African Earth Sciences*, **32**, 765–776.

FEYBESSE, J. L. & & MILÉSI, J. P. 1994. The Archaean/Proterozoic contact zone in West Africa: a mountain belt of d6collement thrusting and folding on a continental margin related to 2.1 Ga convergence of Archaean cratons? *Precambrian Research*, **69**, 199–227.

FROST, B. R., BARNES, C. G., COLLINS, W. J., ARCULUS, R. J., ELLIS, D. J. & FROST, C. D. 2001. A geochemical classification for granitic rocks. *Journal of Petrology*, **42**, 2033–2048.

GASQUET, D., LEVRESSE, G., CHEILLETZ, A., AZIZI-SAMIR, M. R. & MOUTTAQI, A. 2005. Contribution to a geodynamic reconstruction of the Anti-Atlas (Morocco) during Pan-African times with the empasis on inversion tectonics and metallogenic activity at the Precambrian-Cambrian transition. *Precambrian Research*, **140**, 157–182.

GASQUET, D., ENNIH, N., LIEGEOIS, J. P., SOULAIMANI, A. & MICHARD, A. 2008. The Pan-African Belt. *In*: MICHARD, A., CHALOUAN, A. & SADDIQI, O. (eds) *Continental Evolution: The Geology of Morocco. Structure, Stratigraphy, and Tectonics of the Africa-Atlantic-Mediterranean Triple Junction.* Springer Verlag, Lecture Notes in Earth Sciences, **116**.

GUIRAUD, R., BOSWORTH, W., THIERRY, J. & DELPLANQUE, A. 2005. Phanerozoic geological evolution of Northern and Central Africa: an overview. *Journal of African Earth Sciences*, **43**, 83–143.

HEFFERAN, K. P., ADMOU, H., KARSON, J. A. & SAQUAQUE, A. 2000. Anti-Atlas (Morocco) role in Neoproterozoic Western Gondwana reconstruction. *Precambrian Research*, **103**, 89–96.

INGLIS, J. D., MACLEAN, J. S., SAMSON, S. D., D'LEMOS, R. S., ADMOU, H. & HEFFERAN, K. 2004. A precise U–Pb zircon age for the Bleïda granodiorite, Anti-Atlas, Morocco: implications for the timing of deformation and terrane assembly in the eastern Anti-Atlas. *Journal of African Earth Sciences*, **39**, 277–283.

JAHN, B. M., CABY, R. & MONIÉ, P. 2001. The oldest UHP eclogites of the World: age of UHP metamorphism, nature of protoliths and tectonic implications. *Chemical Geology*, **178**, 143–158.

LAVILLE, E., PIQUÉ, A., AMRHAR, M. & CHARROUD, M. 2004. A restatement of the Mesozoic Atlasic rifting (Morocco). *Journal of African Earth Sciences*, **38**, 145–153.

LIÉGEOIS, J. P., CLAESSENS, W., CAMARA, D. & KLERKX, J. 1991. Short-lived Eburnian orogeny in southern Mali. Geology, tectonics, U–Pb and Rb–Sr geochronology. *Precambrian Research*, **50**, 111–136.

LIÉGEOIS, J. P., LATOUCHE, L., BOUGHRARA, M., NAVEZ, J. & GUIRAUD, M. 2003. The LATEA metacraton (Central Hoggar, Tuareg shield, Algeria): behaviour of an old passive margin during the Pan-African orogeny. *Journal of African Earth Sciences*, **37**, 161–190.

LIÉGEOIS, J. P., BENHALLOU, A., AZZOUNI-SEKKAL, A., YAHIAOUI, R. & BONIN, B. 2005. The Hoggar swell and volcanism: reactivation of the Precambrian Tuareg shield during Alpine convergence and West African Cenozoic volcanism. *In*: FOULGER, G. R., NATLAND, J. H., PRESNALL, D. C. & ANDERSON, D. L. (eds) *Plates, Plumes and Paradigms*. Geological Society of America, Special Paper, **388**, 379–400.

LUGMAIR, G. W. & MARTI, K. 1978. Lunar initial $^{143}Nd/^{144}Nd$: differential evolution of the lunar crust and mantle. *Earth and Planetary Science Letters*, **39**, 349–357.

MALUSA, M. G., POLINO, R., FERONI, A. C., ELLERO, A., OTTRIA, G., BAIDDER, L. & MUSUMECI, G. 2007. Post-Variscan tectonics in eastern Anti-Atlas (Morocco). *Terra Nova*, **19**, 481–489.

MARZOLI, A., RENNE, P. R., PICCIRILLO, E. M., ERNESTO, M., BELLIENI, G. & DE MIN, A. 1999. Extensive 200-million-year-old continental flood basalts of the Central Atlantic Magmatic Province, *Science*, **284**, 616–618.

MILLER, C. F., MCDOWELL, S. M. & MAPES, R. W. 2003. Hot and cold granites? Implications of zircon saturation temperatures and preservation of inheritance. *Geology*, **31**, 529–532.

MOUSSINE-POUCHKINE, A. & BERTRAND-SARFATI, J. 1978. Le Gourma: un aulacogène du Précambrien supérieur? *Bulletin de la Société Géologique de France*, **20**, 851–857.

NAVEZ, J. 1995. Détermination d'éléments en traces dans les roches silicatées par ICP-MS. Rapport Annuel du Département de Géologie et Minéralogie 1993–1994 Musée Royal de l'Afrique Centrale, Tervuren, Belgique, 139–147.

NÉDÉLEC, A., AFFATON, P., FRANCE-LANORD, C., CHARRIÈRE, A. & ALVARO, J. 2007. Sedimentology and chemostratigraphy of the Bwipe Neoproterozoic cap dolostones (Ghana, Volta Basin): a record of microbial activity in a peritidal environment. *Comptes Rendus Geosciences*, **339**, 223–239 and erratum *Comptes Rendus Geosciences*, **339**, 516–518.

NELSON, B. K. & DEPAOLO, D. J. 1985. Rapid production of continental crust 1.7 to 1.9 b.y. ago: Nd isotopic evidence from the basement of the North Americam midcontinent. *Geological Society of America Bulletin*, **96**, 746–754.

PATIÑO DOUCE, A. E. 1992. Calculated relationships between activity of alumina and phase assemblages of silica-saturated igneous rocks. *Journal of Volcanology and Geothermal Research*, **52**, 43–63.

PELLETER, E., CHEILLETZ, A., GASQUET, D. *ET AL*. 2007. Hydrothermal zircons: a tool for ion microprobe U–Pb dating of gold mineralization (Tamlalt-Menhouhou gold deposit—Morocco). *Chemical Geology*, **245**, 135–161.

POTREL, A., PEUCAT, J. J. & FANNING, C. M. 1998. Archean crustal evolution of the West African craton: example of the Amsaga area (Reguibat Rise). U–Pb and Sm–Nd evidence for crustal growth and recycling. *Precambrian Research*, **90**, 107–117.

SAMSON, S. D., INGLIS, J. D., D'LEMOS, R. S., ADMOU, H., BLICHERT-TOFT, J. & HEFFERAN, K. 2004. Geochronological, geochemical, and Nd-Hf isotopic constraints on the origin of Neoproterozoic plagiogranites in the Tasriwine ophiolite, Anti-Atlas orogen, Morocco. *Precambrian Research*, **135**, 133–147.

SAMSON, S. D. & D'LEMOS, R. S. 1998. U–Pb geochronology and Sm–Nd isotopic composition of Proterozoic gneisses, Channel Islands, UK. *Journal of the Geological Society, London*, **155**, 609–618.

SOULAIMANI, A, ESSAIFI, A, YOUBI, N. & HAFID, A. 2004. Les marqueurs structuraux et magmatiques de l'extension crustale au Protérozoïque terminal–Cambrien basal autour du massif de Kerdous (Anti-Atlas occidental, Maroc). *Comptes Rendu Geoscience*, **336**, 1433–1441.

STEIGER, R. H. & JÄGER, E. 1977. Subcommission on geochronology: convention on the use of decay constants in geo- and cosmochronology. *Earth and Planetary Sciences Letters*, **36**, 359–362.

THOMAS, R. J., CHEVALLIER, L. P., GRESSE, P. G. *ET AL*. 2002. Precambrian evolution of the Sirwa Window, Anti-Atlas Orogen, Morocco. *Precambrian Research*, **118**, 1–57.

THOMAS, R. J., FEKKAK, A., ENNIH, N. *ET AL*. 2004. A new lithostratigraphic framework for the Anti-Atlas Orogen, Morocco. *Journal of African Earth Sciences*, **39**, 217–226.

VERATI, C., BERTRAND, H. & FERAUD, G. 2005. The farthest record of the Central Atlantic Magmatic Province into West Africa craton: Precise $^{40}Ar/^{39}Ar$ dating and geochemistry of Taoudenni basin intrusives (northern Mali). *Earth and Planetary Science Letters*, **235**, 391–407.

VEKSLER, I. V., DORFMAN, A. M., KAMENETSKY, M., DULSKI, P. & DINGWELL, D. B. 2005. Partitioning of lanthanides and Y between immiscible silicate and fluoride melts, fluorite and cryolite and the origin of the lanthanide tetrad effect in igneous rocks. *Geochimica et Cosmochimica Acta*, **69**, 2847–2860.